The AEgIS experiment

Measuring the gravitational interaction of antimatter

A. Knecht · S. Aghion · O. Ahlén · C. Amsler · A. Ariga · T. Ariga · A. S. Belov · G. Bonomi · P. Bräunig · J. Bremer · R. S. Brusa · L. Cabaret · C. Canali · R. Caravita · F. Castelli · G. Cerchiari · S. Cialdi · D. Comparat · G. Consolati · J. H. Derking · S. Di Domizio · L. Di Noto · M. Doser · A. Dudarev · A. Ereditato · R. Ferragut · A. Fontana · P. Genova · M. Giammarchi · A. Gligorova · S. N. Gninenko · S. Haider · S. D. Hogan · T. Huse · E. Jordan · L. V. Jørgensen · T. Kaltenbacher · J. Kawada · A. Kellerbauer · M. Kimura · D. Krasnický · V. Lagomarsino · S. Lehner · C. Malbrunot · S. Mariazzi · V. A. Matveev · F. Merkt · F. Moia · G. Nebbia · P. Nédélec · M. K. Oberthaler · N. Pacifico · V. Petráček · C. Pistillo · F. Prelz · M. Prevedelli · C. Regenfus · C. Riccardi · O. Røhne · A. Rotondi · H. Sandaker · P. Scampoli · J. Storey · M. A. Subieta Vasquez · M. Špaček · G. Testera · D. Trezzi · R. Vaccarone · E. Widmann · S. Zavatarelli · J. Zmeskal

Published online: 1 July 2014

Proceedings of the 11th International Conference on Low Energy Antiproton Physics (LEAP 2013) held in Uppsala, Sweden, 10–15 June, 2013

A. Knecht (✉) · O. Ahlén · J. Bremer · J. H. Derking · M. Doser · A. Dudarev · S. Haider · L. V. Jørgensen · T. Kaltenbacher
Physics Department, European Organisation for Nuclear Research, 1211 Geneva 23, Switzerland
e-mail: andreas.knecht@cern.ch

S. Aghion · G. Consolati · R. Ferragut · D. Krasnický · F. Moia
Politecnico di Milano, Piazza Leonardo da Vinci 32, 20133 Milano, Italy

S. Aghion · G. Consolati · R. Ferragut · M. Giammarchi · F. Moia · F. Prelz · D. Trezzi
Istituto Nazionale di Fisica Nucleare, Sez. di Milano, Via Celoria 16, 20133 Milano, Italy

C. Amsler · A. Ariga · T. Ariga · A. Ereditato · J. Kawada · M. Kimura · C. Pistillo · P. Scampoli · J. Storey
Albert Einstein Center for Fundamental Physics, Laboratory for High Energy Physics, University of Bern, 3012 Bern, Switzerland

A. S. Belov · S. N. Gninenko · V. A. Matveev
Institute for Nuclear Research of the Russian Academy of Sciences,
Moscow 117312, Russia

G. Bonomi · M. A. Subieta Vasquez
Department of Mechanical and Industrial Engineering, University of Brescia, Via Branze 38,
25133 Brescia, Italy

G. Bonomi · A. Fontana · P. Genova · C. Riccardi · A. Rotondi · M. A. Subieta Vasquez
Istituto Nazionale di Fisica Nucleare, Sez. di Pavia, Via Agostino Bassi 6, 27100 Pavia, Italy

P. Bräunig · M. K. Oberthaler
Kirchhoff Institute for Physics, University of Heidelberg, Im Neuenheimer Feld 227, 69120 Heidelberg,
Germany

R. S. Brusa · L. Di Noto
Dipartimento di Fisica, Università di Trento and INFN, Gruppo Collegato di Trento, Via Sommarive 14,
38050 Povo, Trento, Italy

L. Cabaret · D. Comparat
Laboratoire Aimé Cotton, CNRS, Université Paris Sud, ENS Cachan, Bâtiment 505, Campus d'Orsay,
91405 Orsay Cedex, France

C. Canali · C. Regenfus
Physics Institute, University of Zurich, Winterthurerstrasse 190, 8057 Zurich, Switzerland

R. Caravita · F. Castelli · G. Cerchiari · S. Cialdi
Department of Physics, University of Milano, Via Celoria 16, 20133 Milano, Italy

S. Di Domizio · G. Testera · R. Vaccarone · S. Zavatarelli
Istituto Nazionale di Fisica Nucleare, Sez. di Genova, Via Dodecaneso 33, 16146 Genova, Italy

A. Gligorova · N. Pacifico · H. Sandaker
Institute of Physics and Technology, University of Bergen, Alleegaten 55, 5007 Bergen, Norway

S. D. Hogan
Department of Physics and Astronomy, University College London,
Gower Street, London WC1E 6BT, UK

T. Huse · O. Røhne
Department of Physics, University of Oslo, Sem Sælands vei 24, 0371 Oslo, Norway

E. Jordan · A. Kellerbauer
Max Planck Institute for Nuclear Physics, Saupfercheckweg 1, 69117 Heidelberg, Germany

V. Lagomarsino
Department of Physics, University of Genoa, Via Dodecaneso 33, 16146 Genova, Italy

S. Lehner · C. Malbrunot · S. Mariazzi · E. Widmann · J. Zmeskal
Stefan Meyer Institute for Subatomic Physics, Austrian Academy of Sciences,
Boltzmanngasse 3, 1090 Vienna, Austria

V. A. Matveev
Joint Institute for Nuclear Research, 141980 Dubna, Russia

F. Merkt
Laboratory for Physical Chemistry, ETH Zurich, 8093 Zurich, Switzerland

G. Nebbia
Istituto Nazionale di Fisica Nucleare, Sez. di Padova, Via Marzolo 8, 35131 Padova, Italy

1 Introduction

The Weak Equivalence Principle (WEP) is one of the foundations of General Relativity. It postulates that the trajectory of a point mass in the presence of gravity is independent of its composition and depends only on its initial position and velocity. While the WEP has been tested by Etvös-type experiments with precisions down to the 10^{-13} level [1], no direct tests have been performed with antimatter. Measurements with positrons and antiprotons have been attempted but failed due to interferences of electromagnetic fields. With the recent developments in the production of large amounts of cold, neutral anihydrogen [2, 3] at CERN's Antiproton Decelerator (AD) [4] such measurements have now become feasible.

Many arguments have been put forward to constrain potential differences between the acceleration of antimatter $\bar{g}$ and matter g both on theoretical grounds but also from indirect measurements. However, just as many arguments have been put forward refuting the validity of such constraints (see, e.g., [5, 6] for a summary). Thus at this point scenarios with only small differences between g and $\bar{g}$ or so-called "antigravity" with $\bar{g} = -g$ are still conceivable.

At this point it thus falls on direct measurements to test the validity of the WEP for the antimatter sector. A first test with antihydrogen has been attempted recently [7]. The AEgIS collaboration [8] aims at performing the first conclusive measurement of $\bar{g}$ with an initial precision of 1 %. Another experiment, GBAR [9], has been approved and is due to start operation at the new very low energy antiproton ring ELENA in 2018.

In the following sections the AEgIS experiment and its current status will be discussed.

2 Experimental principle

The basic principle of the AEgIS experiment can be seen in Figs. 1 and 2. After the capture of antiprotons from the AD they are cooled down to the lowest temperature possible. Positrons captured from a strong ^{22}Na source are brought to the same environment. From this central trap the positrons are displaced off-axis using the auto-resonant technique of exciting the collective diocotron mode of the plasma [10, 11]. Subsequently the positrons are launched from this off-axis trap onto a porous silica target thereby forming positronium [12]. The positronium that diffuses out of the porous silica into vacuum is hit by two

P. Nédélec
Institut de Physique Nucléaire de Lyon, Claude Bernard University Lyon 1, 4 Rue Enrico Fermi, 69622 Villeurbanne, France

V. Petráček · M. Špaček
Czech Technical University in Prague, FNSPE, Břehová 7, 11519 Praha 1, Czech Republic

M. Prevedelli
Department of Physics, University of Bologna, Via Irnerio 46, 40126 Bologna, Italy

C. Riccardi · A. Rotondi
Department of Nuclear and Theoretical Physics, University of Pavia, Via Bassi 6, 27100 Pavia, Italy

P. Scampoli
Department of Physics, University of Napoli Federico II, Via Cinthia, 80126 Napoli, Italy

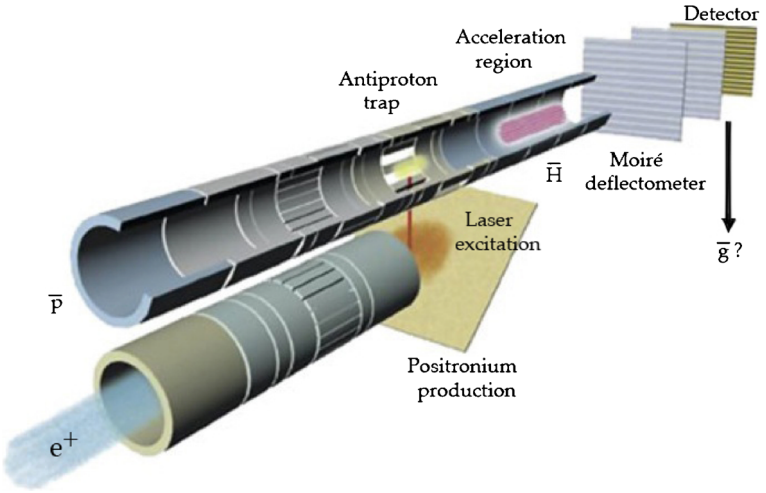

Fig. 1 Overview of the experimental principle: Positrons are converted into positronium in a porous silica target. The laser-excited positronium interacts with the antiprotons forming antihydrogen via a charge-exchange reaction. The Rydberg antihydrogen atoms are Stark accelerated and directed towards a moiré deflectometer. The deflectometer is used to extract the gravitational acceleration for antimatter $\bar{g}$

superimposed laser beams exciting the positronium in a two-step process to states with principal quantum numbers n_{Ps} of around 30 [13]. The exact state can be chosen by tuning the laser frequency and will have to be optimized experimentally.

The excited positronium expands through a semitransparent trap and interacts with the antiprotons forming antihydrogen via a charge-exchange reaction:

$$Ps^* + \bar{p} \rightarrow \bar{H}^* + e^- \tag{1}$$

A variation of this technique has been tested in Ref. [14]. The advantages of this antihydrogen formation mechanism are threefold: i) The reaction cross section is large and scales with the fourth power of n_{Ps}. ii) The final state distribution of the produced antihydrogen is narrow and defined by n_{Ps}. For $n_{Ps} = 35$ the corresponding $n_{\bar{H}}$ is around 45. iii) Antihydrogen is produced from antiprotons at rest. The kinetic energy of the antihydrogen is determined by the temperature of the antiproton cloud.

Right after the production of antihydrogen the trap potentials are set such as to form a strong gradient electric field. The antihydrogen are Stark accelerated through the interaction of the large dipole moment of the Rydberg atom with the gradient field [15]. Typically the antihydrogen atoms will be accelerated to axial velocities of around 400 m/s. The radial velocities will be determined by the temperature of the antiproton cloud. For a temperature of 100 mK this amounts to approximately 50 m/s. The achievable temperature of the antiproton cloud affects the experiment in two ways: i) At higher temperatures the antihydrogen beam becomes more divergent and thus less antihydrogen atoms reach our detector. ii) The production rate of antihydrogen is reduced at higher temperatures. While reaching 100 mK is the goal of the apparatus the gravity measurements are – to our best current knowledge – still feasible at temperatures of a few Kelvin.

The final result of all these steps above is thus the production of a pulsed, cold antihydrogen beam. The antihydrogen beam will be directed towards a moiré deflectometer (see Fig. 2 (right)) which cuts the broad, uncollimated distribution of incoming antihydrogen

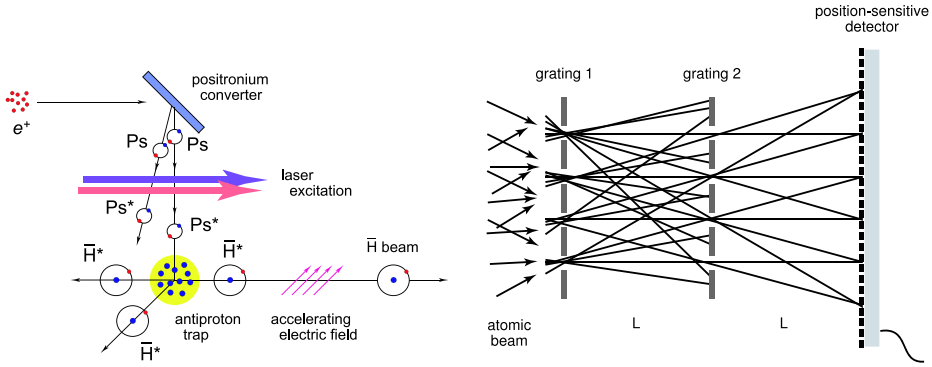

Fig. 2 *Left*: Schematic of the charge-exchange reaction with positronium. The positronium is laser excited and interacts with the antiproton cloud through the reaction $Ps^* + \bar{p} \rightarrow \bar{H}^* + e^-$. The resulting Rydberg antihydrogen is accelerated in a gradient electric field forming an antihydrogen beam.
Right: Principle of the moiré deflectometer. The incoming broad and divergent beam is chopped through two gratings acting as shadow masks into a narrow fringe pattern which is recorded with a position-sensitive detector

atoms into a narrow fringe pattern that can be imaged with a position-sensitive detector. Any acceleration over the flight path between the first grating and the detector will lead to a displacement of the imaged fringe pattern. In the case of gravity the displacement is given by

$$\Delta x = \bar{g}\frac{L^2}{v^2} = \bar{g}t^2 \tag{2}$$

with the grating length L, the velocity of the antihydrogen atom v and the time-of-flight t. Thus by registering for each antihydrogen its time-of-flight after production and vertex on the position-sensitive detector, the gravitational acceleration $\bar{g}$ for antimatter can be extracted.

3 Experimental apparatus

The AEgIS experiment is located at the antiproton decelerator (AD) at CERN. The main components of the experimental apparatus can be seen in Fig. 3. Typically every ~100 s the AD delivers 3×10^7 antiprotons at an energy of 5.3 MeV to experiments. The energy of the antiprotons is further degraded by inserting thin foils of aluminum and a silicon beam counter into their path. Out of the 3×10^7 antiprotons typically 120 000 can be captured. For this purpose the stack of traps inside the 5 T magnet features three high-voltage electrodes tested up to 12 kV that can be used for the capture, storage and cooling both of antiprotons and positrons. The 1 T magnet houses the ultracold traps used for the final cooling of the antiprotons before antihydrogen formation and the off-axis traps used for launching the positrons onto the positronium formation target.

Around the formation region a scintillating fibre detector is installed. It operates 800 scintillating fibers at 4K each individually sampled at 200 MHz [16]. From the hit pattern antiproton annihilation vertices can be reconstructed with ~2 mm resolution.

The positrons are delivered from a 800 MBq ^{22}Na source covered with a solid neon moderator. Positrons are first trapped and then loaded into a buffer gas filled accumulator.

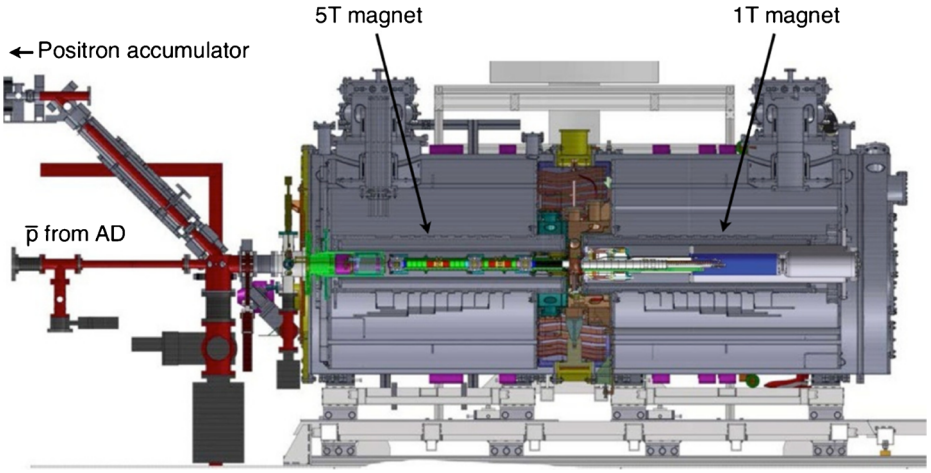

Fig. 3 The AEgIS experimental apparatus. Antiprotons and positrons are delivered from the left from the AD and the positron accumulator, respectively. They are captured within the traps inside the 5 T magnet and then brought to the 1 T magnet for the formation of antihydrogen. The downstream deflectometer region has yet to be designed and built

A pulsed transfer line of ∼0.1 T guides the positrons down from the accumulator into the 5 T traps.

Apart from the downstream deflectometer region all the major experimental components have been built and installed. Figure 4 shows an overview of the apparatus as of December 2012.

4 Commissioning results

Initial commissioning with antiprotons had been carried out in May/June 2012 with only the 5 T magnet installed [17]. In December 2012 the equipment as shown in Fig. 4 was ready and could be used to perform tests using electrons, antiprotons and positrons.

The antiproton system behaved as expected and the relevant parameters could be determined in order to trap the largest amount of antiprotons. These were the variation of the thickness of the degrader foils at the entrance of the 5 T cryostat, the high-voltage applied to the catching electrodes and the timing for switching the high-voltage electrodes after the extraction of the antiproton bunch from the AD. Typically 120 000 antiprotons were captured. In addition, the cooling of the antiprotons with a pre-loaded cloud of electrons was studied.

Due to a very fast pump-down, bake-out and cool-down of the apparatus the vacuum levels were not at its optimal pressure but low enough to allow for lifetimes of cold antiprotons of ∼500 s. This was long enough to manipulate the antiproton cloud inside the traps and test more advanced procedures such as stacking of antiprotons. For this antiprotons are captured and cooled into a small potential well. While holding on to the cooled antiprotons the next shot of antiprotons from the AD is again captured and cooled into the same well. The antiproton bunches are thus “stacked” on top of each other. Limited only by the lifetime of the antiprotons inside the trap, stacks of 5 AD shots could be built without any problems.

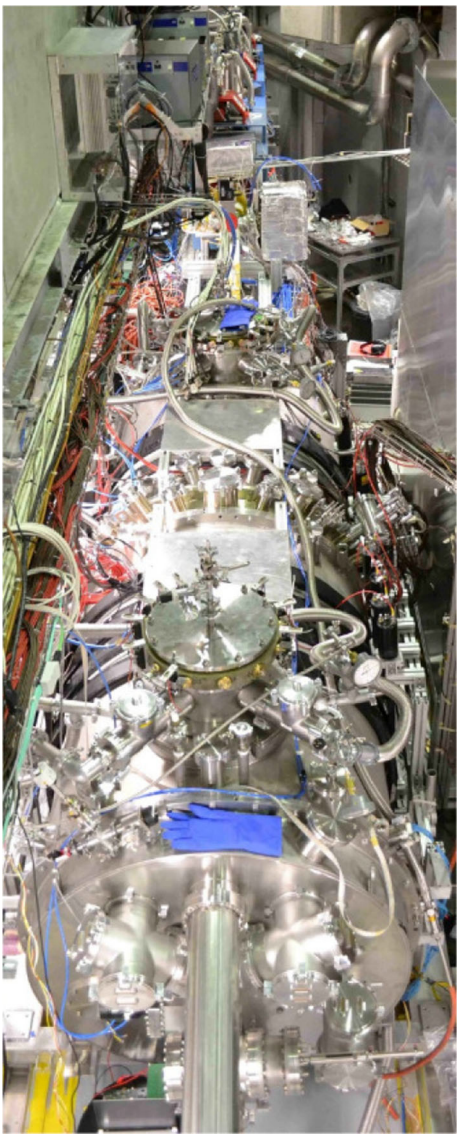

Fig. 4 Picture of the experimental apparatus. Visible in the front is the cryostat of the 1 T magnet followed by the 5 T magnet. All the way in the back the positron accumulator is visible within its blue frame. The metal plate on the right constitutes part of the enclosure for the laser installation used for positronium excitation. The black bands around the cryostats are large plastic scintillators used to detect antiproton annihilations along the traps

While not yet at its optimal efficiency the accumulator delivered approximately 8×10^6 positrons per shot (approximately a factor of 20 below of its design value of 10^8 positrons per shot). With this intensity the pulsed transfer line bringing the positrons from the accumulator to the traps in the 5 T magnet was tuned. Approximately 80 % of the accumulated positrons were transported through the transfer line into the 5T magnet. The critical points (vacuum level in accumulator, alignment of magnetic fields) have been identified and efforts to achieve lossless transport are ongoing. Scintillators positioned around the cryostats could be used to track the passage of the positrons through the 5 and 1 T traps. Figure 5 shows the signal sent to the accumulator to release a the positrons and the response of two scintillators around the 1 T cryostat as the positrons annihilate in that region.

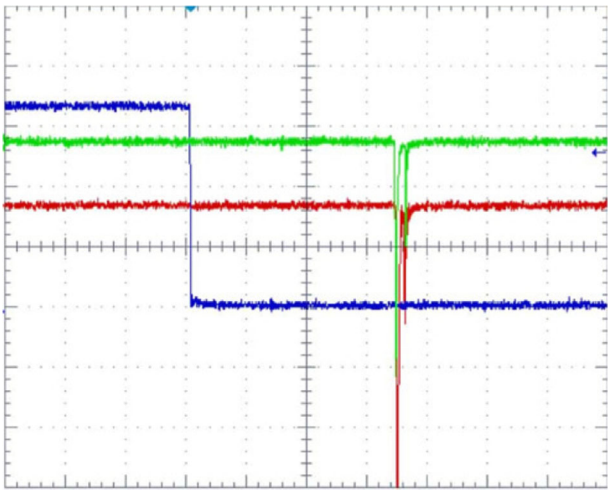

Fig. 5 Oscilloscope traces for the signal sent to the positron accumulator to dump positrons (*blue, rectangular*) and the response of two scintillators mounted on the 1 T cryostat registering the annihilation of the positrons in that area

5 Detector tests

During the beam time in December 2012 a six-way cross was mounted at the end of the 1 T magnet at the position of a future deflectometer setup. The six-way cross was separated from the cryostats with a valve and could be used for detector tests with a rapid turnaround time. The detector tests were performed in a parasitic mode profiting from the fact that only a small fraction of antiprotons are captured in the trap while the rest of the antiprotons – typically still around 10^7 – are guided through the cryostats due to the strong magnetic field. Typical energy of the antiprotons at this point is around 100 keV arriving at the six-way cross as a bunch of around 110 ns in length. More details on some of the detector tests can be found in Ref. [18].

5.1 Nuclear emulsions

We have tested various nuclear emulsion detectors [19] in different configurations to assess their suitability as the position-sensitive detector for the deflectometer. After the exposure the emulsions are developed in a dark room and scanned by automated microscopes. A typical result, reaching vertex resolutions of about 1 μm, can be seen in Fig. 6 (left). A more detailed description of the results obtained and the implication for its use with the moiré deflectometer is available in Ref. [20] and is presented as well in these proceedings [21].

5.2 Microchannel plates

We have tested two detector systems based on a microchannel plate (MCP). In the first test the MCP was exposed directly to the antiproton beam. The MCP was readout by a phosphor screen and camera assembly. Due to the large divergence of the beam in the stray field of

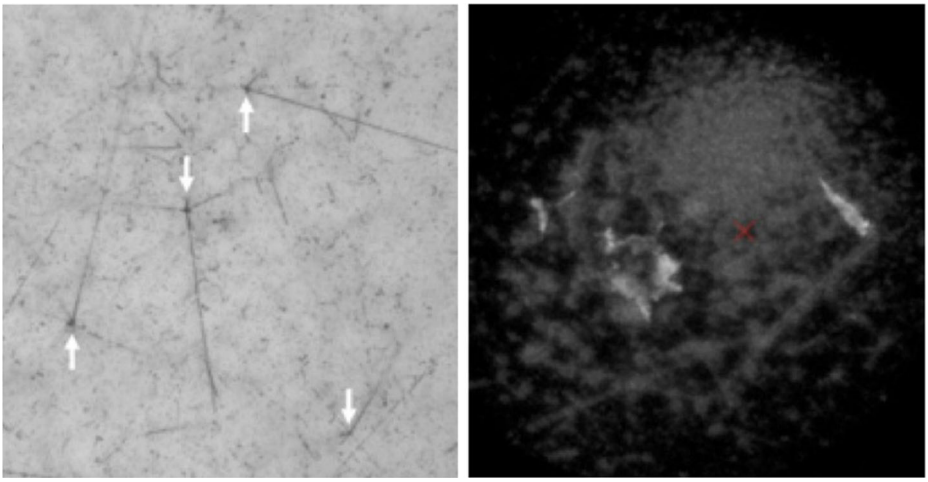

Fig. 6 *Left*: Processed image of a bare emulsion exposed to antiprotons. The arrows mark the vertices of antiproton annihilations. *Right*: Image taken with a microchannel plate together with a phosphor screen and camera readout. The bright spots are damages on the phosphor screen

the 1 T magnet the MCP was almost uniformly illuminated. Additionally, due to the large number of antiprotons impinging on the detector it was only possible to discern individual antiproton annihilations at the edges of the plate where the occupancy was slightly less. A typical example of an image taken with a single shot of antiprotons from the AD is shown in Fig. 6 (right).

In the second test, a thin aluminum foil biased at -10 kV was exposed to the antiproton beam. Emitted secondary electrons were accelerated onto the MCP and imaged as above. The resulting images were slightly "cleaner" due to the absence of thick tracks on the MCP. More details can be found in Ref. [18].

5.3 Silicon detectors

Various silicon detectors were tested by exposing them directly to the antiprotons. A typical setup can be seen in Fig. 7 (left). Among the detectors tested was a 3D pixel sensor designed for the ATLAS upgrade, a strip sensor and the Mimotera detector. The Mimotera detector is an ultra-thin pixel detector with 15 μm active depth. The analysis of the results with these detectors also allows for a detailed comparison between the data and Monte Carlo simulations of the annihilation properties of low energy antiprotons on bare silicon. A publication describing the results achieved with the Mimotera detector is in preparation. The results obtained with the other two detector systems are currently still under analysis.

5.4 Miniature Moiré deflectometer

In order to assess the performance of one of the critical components of the experiment we have built a miniature moiré deflectometer. A picture of the structure holding the silicon gratings can be seen in Fig. 7 (right). Behind the deflectometer we installed an emulsion

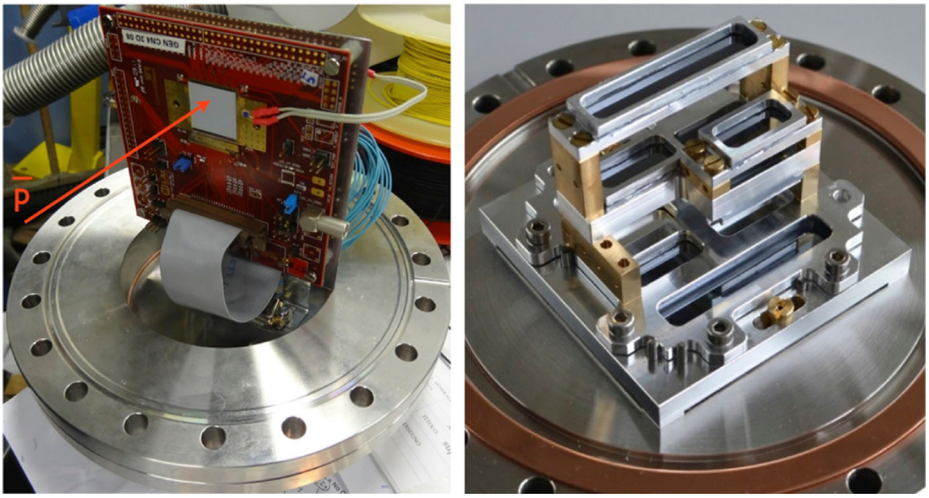

Fig. 7 *Left*: Setup for the tests of silicon detectors exposed directly to antiprotons. *Right*: Miniature moiré deflectometer mounted on top of an emulsion detector. The structure provides the holders for the different silicon gratings

detector and exposed the setup for 7 hours to antiprotons. After the development and digitization of the emulsion we successfully detected the antiproton fringes in the annihilation vertices with the correct period of 40 μm as given by the grating structure. In addition, we have aligned the deflectometer using light and a part of the structure where only a single grating is present. This will allow to determine potential forces that acted on the antiprotons during their flight through the deflectometer. The corresponding publication is in preparation.

6 Conclusions and outlook

The AEgIS experiment has made good progress on its way to the first measurement of the gravitational acceleration of antimatter. Large parts of the apparatus are installed and could be taken into operation for the first time in December 2012.

Parasitic detector and deflectometer tests were conducted during the same beam time of December 2012 and provided essential input into the design and construction of the deflector setup needed to perform the gravity measurement.

During the period of the long-shutdown (LS1) at CERN, when no antiprotons are available, a proton source will be installed on the apparatus to refine the necessary procedures for the production of antihydrogen by exploiting the charge symmetry of the reaction (1).

Acknowledgments We wish to warmly acknowledge our technical collaborators Luca Dassa, Roger Hänni and Jacky Rochet without whom the experiment could not have been built. E.W. wishes to acknowledge the support by the European Research Council Grant No. 291242-HBAR-HFS and the Austrian Ministry for Science and Research.

References

1. Adelberger, E.G. et al.: Progr. Part. Nucl. Phys. **62**, 102 (2009)
2. Amoretti, M. et al.: Nature **419**, 456 (2002)
3. Gabrielse, G. et al.: Phys. Rev. Lett. **89**, 213401 (2009)
4. Hémy, J.Y., Maury, S.: Nucl. Phys. A **655**, 345c (1999)
5. Nieto, M.M., Goldman, T.: Phys. Rep. **205**, 221 (1991)
6. Fischler, T.R.M., Lykken, J.: Tech. Rep. FERMILAB-FN-0822-CD-T, Fermi National Laboratory (2008)
7. Charman, A.E. et al.: Nat. Commun. **4**, 1785 (2013)
8. AEgIS collaboration. http://aegis.web.cern.ch
9. GBAR collaboration. http://gbar.in2p3.fr
10. Danielson, J.R. et al.: Phys. Plasmas **13**, 123502 (2006)
11. Canali, C. et al.: Eur. Phys. J. D **65**, 499 (2011)
12. Mariazzi, S. et al.: Phys. Rev. B **81**, 235418 (2010)
13. Cialdi, S. et al.: Nucl. Instr. Meth B **269**, 1527 (2011)
14. Storry, C.H. et al.: Phys. Rev. Lett. **93**, 263401 (2004)
15. Vliegen, E., Merkt, F.: J. Phys. B: At Mol. Opt. Phys. **39**, L241 (2006)
16. Storey, J., et al.: Nucl. Instr. and Meth. A (in press) (2013)
17. Krasnický, D. et al.: AIP Conf. Proc. **1521**, 144 (2012)
18. Sosa, A., et al.: (in these proceedings) (2013)
19. de Lellis, G., Ereditato, A., Niwa, K.: in *Springer Materials, Landolt-Börnstein Database* (http://www.springermaterials.com), ed. by C.W. Fabjan, H. Schopper (Springer-Verlag, Heidelberg, 2011)
20. Aghion, S. et al.: J. Instrument. **8**, P08013 (2013)
21. Storey, J., et al.: (in these proceedings) (2013)